Oxidation Behavior of AISI 430 Ferritic Stainless Steel Coated with Ni-Co-TiO_2

Z. Zhaleh [1], M. Zandrahimi [*2], H. Ebrahimifar [3]

[1, 2] Department of Metallurgy and Materials Science, Faculty of Engineering, Shahid Bahonar University of Kerman, Kerman, Iran.
[3] Department of Materials Engineering, Faculty of Mechanical and Materials Engineering, Graduate University of Advanced Technology, Kerman, Iran.

Abstract

Ferritic stainless steels are used in high- temperature applications like solid oxide fuel cells. Application of steels in these conditions will expose them to severe thermal cycles. Therefore, it is essential to protect them at high temperatures. One of the most effective methods for increasing the life of these components against oxidation is to utilize composite and ceramic coatings. In the present study, Ni-Co-TiO2 composite coating was deposited on AISI 430 steel substrate by electroplating to investigate the oxidation behavior at the operating conditions of solid oxide fuel cells. To observe the morphology, scanning electron microscopy (SEM) and to determine the phases, X-ray diffraction (XRD) were employed. For investigating the oxidation behavior of steel isothermal and cyclic oxidation tests were performed at 800 °C on the samples. Results showed that in isothermal and cyclic oxidation tests, due to the formation of Ni-Co spinel's, coated samples showed less weight gain than uncoated samples. Spinel prevented outward Cr diffusion which improved the oxidation resistance of AISI 430 steel.

Keywords: Oxidation; AISI 430 ferritic stainless steel; Ni-Co-TiO_2 Composite Coating; Electroplating.

1. Introduction

As the operating temperature of solid oxide fuel cell (SOFC) reduces to below 800 ºC, metallic alloys can be used as the interconnect material. Metallic interconnect offers many advantages over ceramic interconnect such as high thermal and electrical conductivity, good ductility, and low cost of raw materials and fabrication. Cr_2O_3-forming alloys, such as Ebrite, Crofer- 22APU and Haynes 230 are promising candidates for the interconnect applications as they form a thin protective layer of Cr_2O_3 scale on the alloy surface upon thermal exposure. Ferritic Cr_2O_3-forming alloys are especially attractive because of their low cost and they closely match the coefficient of thermal expansion (CTE) with other fuel cell components. One major concern with these alloys is their long-term stability and compatibility with other fuel cell components as a result of continuous Cr_2O_3 scale growth [1–3] and Cr migration to the cathode side through gaseous Cr-cations [4]. While the Cr_2O_3 scale growth increases the area-specific resistance (ASR) of the oxide scale, the migration of Cr species to the cathode side can cause the

* *Corresponding author*
Email: M.Zandrahimi@uk.ac.ir
Address: Department of Metallurgy and Materials Science, Faculty of Engineering, Shahid Bahonar University of Kerman, Kerman, Iran.
1. M.Sc.
2. Professor
3. Assistant Professor

degradation of the cathode performance during cell operation [5, 6].

One of the most effective approaches to improve the interconnect properties is to apply surface coatings to provide better conductivity, reduced scale growth and Cr volatility. Recent researches, however, have concentrated on the application of protective/conductive coatings. Numerous techniques have been developed to apply coatings to ferritic stainless steels [7-15].

Among methods for construction composite coatings, electroplating is a significant production method, because it has the advantages of uniform deposition on complexly shaped substrates, low cost and homogeneous distribution of particles [16].

Due to the wide application of nickel as a protective coating, nickel composite coatings containing ceramic particles such as TiO_2 [16-18], Al_2O_3 [19-21], SiC [21-25], CeO_2 [26], SnO_2 [27], TiB_2 [28], Fe_2O_3 [29-31] have been considered mostly in the literature.

Khoran et al. investigated the addition of TiO_2 oxide on microstructure and oxidation behavior of Ni-TiO_2 composite coating. Their results showed that by addition of TiO_2 oxide to nickel coating, grain size decreased and the oxidation behavior improved [16].

Zhang and his colleagues [26] investigated the properties, structure and thermal stability of Ni-Co composite coatings containing CeO_2 nanoparticles. Their results showed that composite coatings had greater microhardness and thermal stability than Ni-Co coatings without cerium oxide. They investigated the oxidation of A3 carbon steels deposited with Ni and Ni-CeO_2 films at 900°C. The results of their investigation showed that the oxidation rate of Ni-CeO_2 coatings was lower than that of the coatings with Ni and the uncoated samples [26].

Geng et al. found out that the oxidation behavior of the AISI 430 stainless steel did not improve by adding the Ni-Fe_2O_3 coating, whatever its oxidation kinetic after one week was the same as the bare steel [29].

So far, electroplating method has not been employed for coating of AISI 430 steel with Ni-Co-TiO_2 composite.

In this research, Ni-Co-TiO_2 composite was coated on AISI 430 steel substrate by electroplating plating method. Microstructure and surface morphology were revealed by scanning electron microscopy (SEM). X-ray diffraction (XRD) was employed to specify the formed phases. Isothermal and cyclic oxidation tests were performed at 800 °C to study the oxidation behavior of uncoated and coated steels.

2. Experimental Procedure

Samples of AISI 430 with dimensions of 10 × 10 mm × 2 mm were used as coating substrates and pure nickel sheet (99% purity) with a dimension of 20 × 20 mm × 20 mm as an anode. Chemical composition of AISI 430 steel is shown in Table. 1. Preparation of the samples before plating according to the ASTM B254 standard was carried out. Steel plates with 400, 600, 800, 1200 and 2500 sandpapers were polished and the washing operation was done using soap and water. The samples were placed in an ultrasonic device for 10 minutes in acetone. Then the samples were washed with distilled water and in the final step, the surface activation in 10% sulfuric acid solution was done for 90 seconds. Samples were placed in the electrolyte solution immediately after preparation.

Table. 1. Chemical composition of AISI 430 stainless steel (in wt. %).

Cr	Mn	Si	C	P	S	Fe
17.4	1.6	1	0.12	0.03	0.02	balance

Chemical compositions and operating conditions for electrodeposition are given in Table. 2. All chemicals were analytic grade reagents (Merck). Contents of the electrolyte bath were given sonication for about 15 min in order to break down agglomerates. Also, during electrodeposition, agglomeration of particles was prevented by a magnetic stirrer. The stirring speed was 80 rpm.

Table 2. Composition of coating mixtures and electrodeposition parameters/materials.

Coating mixtures		Electrodeposition parameters/materials	
$NiSO_4.6H_2O$	200.00 g/L	Current density	15 mA.cm^{-2}
$NiCl_2.6H_2O$	40.00 g/L	pH	4.5
$CoSO_4.7H_2O$	30.00 g/L	string speed	400 rpm
H_3BO_3	30.00 g/L	Plating time	20 min
TiO_2	20.00 g/L	Plating temperature	50 °C
		Cathode	AISI 430 stainless steel
		Anode	Nickel plate

In this operation, the bathroom components were first weighed down by the GF-300 digital scale and then reached 100 milliliters by adding distilled water. The ALFA-HS860 was used to mix better material from a magnetic stirrer. The PROVA 8000 was used to generate electricity from the power supply. The solution pH was adjusted using sulfuric acid or sodium hydroxide, and the AZ 8686 pH meter was used to control the pH.

In order to prevent the agglomeration of TiO_2 powders, TiO_2 powders were dispersed ultrasonically in solution for 30 min before electrodeposition. During the electrodeposition, magnetic stirring was employed to maintain the uniform particles concentration and prevent the agglomeration.

After electrodeposition the applied current was turned off and the substrate was removed from the electrolyte bath. In order to remove the loosely bound extraneous material from the coated surface, it was washed with distilled water in the ultrasonic instrument. After rinsing with distilled water, the coated steel was dried in air and then weighed using an electronic balance.

In order to evaluate the oxidation behavior, the coated and uncoated specimens were subjected to isothermal oxidation. This test was performed in static air at 800 °C for 200 hours by employing 9 uncoated and 9 coated samples with weight measurement after 5, 10, 20, 40, 60, 80, 100, 150, and 200 hours. Cyclic oxidation at 800 °C up to 50 cycles was exerted to uncoated and coated steel and each cycle consisted of 60 min of heating and 10 min of cooling in air. Mass measurement of uncoated and coated steel before and after oxidation was conducted using a scale with accuracy of 0.0001 gr.

Cross-section microstructure and chemical composition of specimens before and after oxidation were analyzed. The techniques used to characterize the structure and composition of tested specimens included scanning electron microscopy (SEM) (Tscan MV2300) with energy dispersive spectroscopy (EDS) and X-Ray diffraction (XRD) with a Philips X'Pert High Score diffractometer using Cu Kα (λ = 1.5405 Å). The step angle and time step set 0.02° and 1 sec/degree, respectively in all the measurements.

3. Results and discussion

3. 1. Microstructure of Ni-Co-TiO_2 coating

Fig. 1 shows surface morphology and EDS point analysis of a Ni-Co-TiO_2-coated sample. The formed coating is uniform and dense. According to the surface image, the coating is uniform and almost no porosity or agglomeration is visible. EDS analysis represents that the coating mainly consists of Ni, Co, Ti, Fe and O. Analysis by EDS indicated that Ni, Co, Ti, Fe and O contents in the composite coating were 45.9, 37.7, 6.9, 4.4 and 5.1 wt. %, respectively. The amount of TiO_2 was about 8.6 wt. %. The thickness of the composite coating layer was about 4 μm. Fe picks in EDS analysis was because of low thickness of coating. The XRD analysis of the composite coating of Ni-Co-TiO_2 is shown in Fig. 2 as seen from the figure, Ni, Co and TiO_2 phases are existed.

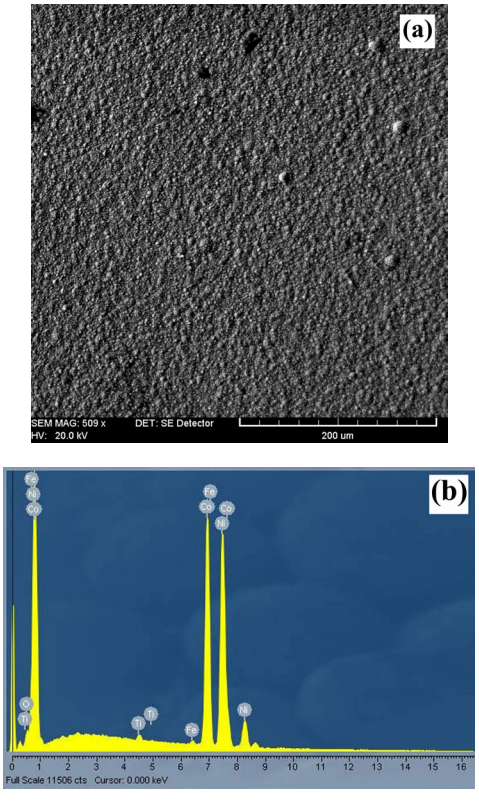

Fig. 1. Surface morphology (a) and EDS analysis (b) as Ni-Co-TiO_2 composite coated sample.

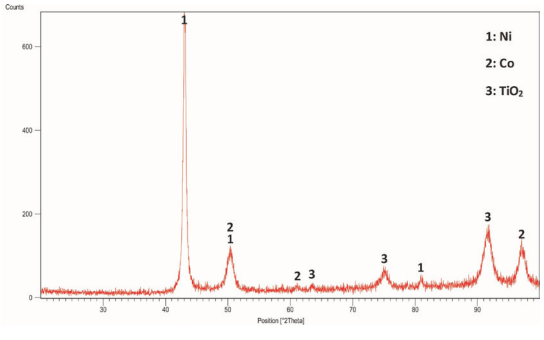

Fig. 2. XRD pattern of Ni-Co-TiO_2-coated sample.

3. 2. Isothermal oxidation behavior

The oxidation behavior of uncoated samples at 800 °C, which was oxidized for 200 hours under the isothermal oxidation, is shown in Fig. 3. After a period of 200

hours of oxidation, the weight gain of uncoated samples was 2.052 mg.cm^{-2}. As shown in Fig. 3, the initial weight gain for uncoated steel until the first 20 hours of oxidation is rapid. This is because of non-protective surface which was seen in the previous researches [14, 15]. After that, the weight gain increased slightly with the oxidation time during second stage (20-200 hours). The slight oxidation rate in this stage was due to the formation of the protective scale (Cr_2O_3), which is consistent with the previous works [32, 33].

When chromium containing stainless steel is exposed to the oxidizing atmosphere, chromium will oxidize and Cr_2O_3 protective scale will form. Over time, the oxidation rate decreases due to Cr_2O_3 scale formation. With the progress of oxidation at high temperatures, the Cr_2O_3 layer will evaporate at the operating conditions of SOFCs, and poisoning of SOFC cathodes will happen.

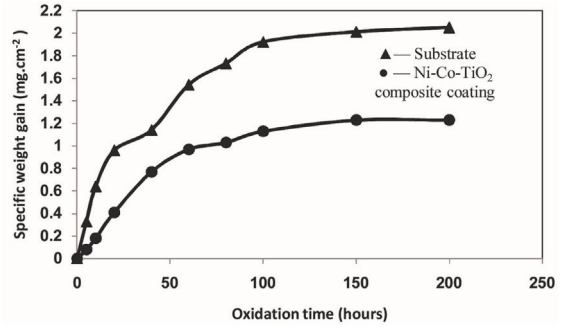

Fig. 3. Weight gain for uncoated and Mn-Co-CeO_2 coated samples as a function of time during isothermal oxidation.

Evaporation of Cr-containing species at high temperature (600–800 °C) [6, 34] is based on the following reactions [6, 13]:

$$Cr_2O_3(s) + 3/2O_2(g) = 2CrO_3(g) \quad (1)$$
$$Cr_2O_3(s) + 2H_2O(g) + 3/2O_2(g) = 2CrO_2(OH)_2(g) \quad (2)$$

Chromium oxide is a type of P-oxide that grows through the migration of chromium cations to the outside. During long-term oxidation or high temperature oxidation, vacant cationic sites move inwards and accumulate in the region of the metal-oxide-interlayer region, causing the cavity and porosity in the region, and therefore decrease the adhesion of the scale to the substrate [14, 15].

For the coated samples, as can be seen, the initial weight gain of the specimens during the first 60 hours of oxidation was high and then the weight gain continued at a lower rate. After 200 hours of the oxidation, the weight gain of the coated samples was 1.229 mg.cm^{-2}.

The weight gain of the coated steel was lower than that of the bare steel. The high weight gain of the coated steel at the first stage (0-60 hrs) was due to the oxidation of the Ni-Co-TiO_2 composite coating. After the 60 hours of oxidation, the weight gain of the coated steel increased slowly with oxidation time. In this stage, oxidation kinetics was slower, implying a protective oxide scale formation between the substrate and the surface oxides developed during oxidation [29, 32].

Fig. 4 shows the square of the weight gain versus time of oxidation for uncoated and Ni-Co-TiO_2 coated AISI 304 stainless steel oxidized at 800 °C. The weight gain of uncoated samples increased parabolically with increasing isothermal oxidation time, which fits the parabolic kinetics law:

$$\left(\frac{\Delta W}{A}\right)^2 = k_p t \quad (3)$$

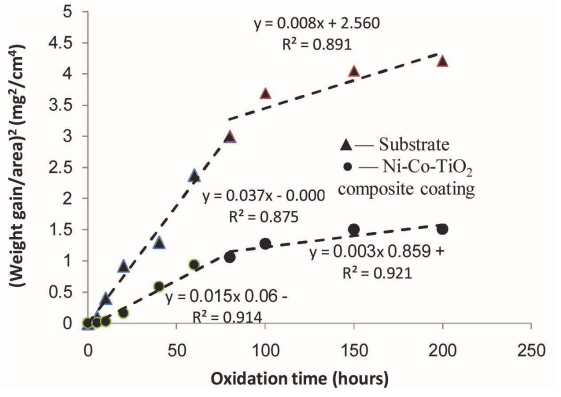

Fig. 4. Square of weight gain as a function of oxidation time in isothermal oxidation for Ni-Co-TiO_2 coated and uncoated samples.

Where ΔW is the weight gain, A is the surface area of the sample, kP is the parabolic rate constant, and t is oxidation time. The parabolic behavior for uncoated and Ni-Co-TiO_2 coated coupons is due to growth of chromia (Cr_2O_3) scale which followed the parabolic rate law [34].

Two oxidation stages are seen in both sample types. According to the parabolic rate law [34-36], the value of kp for uncoated steel during the first stage (between 0 and 60 h) and the second stage (between 60 and 200 h) stages were 9.722 × 10-12 g^2 cm^{-4} s^{-1} and 5.555 ×10 $^{-13}$ g ^{2}cm $^{-4}$s $^{-1}$, respectively. For composite-coated samples, kp was calculated to be 4.111×10-12 g^2 cm^{-4} s^{-1} from 0-60 h. Based on the oxidation kinetics, a protective oxide scale was thermally formed between the substrate and the oxidized coating created during the first oxidation stage [34] .The square of weight gained as a function of oxidation time for the Ni-Co-TiO_2 composite coating from 60-200 h was 2.111×10^{-13} g^2 cm^{-4} s^{-1}, which is lower than during the initial oxidation. It can be concluded that the Ni-Co-TiO_2 composite coating is a protective layer after initial oxidation. The lower Kp value for Ni-Co-TiO_2 coated samples (3.333×10-13 g^2 cm^{-4} s^{-1}) than uncoated samples

(5.555×10^{-13} g^2 cm^{-4} s^{-1}) during the second stage of oxidation implies that diffusion of ions was limited by the Ni-Co-TiO_2 composite coating layer.

The surface morphology of the base alloy at two magnification of 2000X (Fig. 5a) and 4000X (Fig. 5b) and EDS point analysis (c) after 200 hours of oxidation at 800 °C are shown in fig. 5. As can be seen an oxide layer is formed on the surface of the samples. EDS analysis (Fig. 5c) shows that the oxide scale consists of Mn, Cr, Fe and O. Analysis by EDS indicated that Mn, Cr, Fe and O contents in the composite coating were 30.4, 26.5, 21.3 and 21.8 wt.%, respectively.

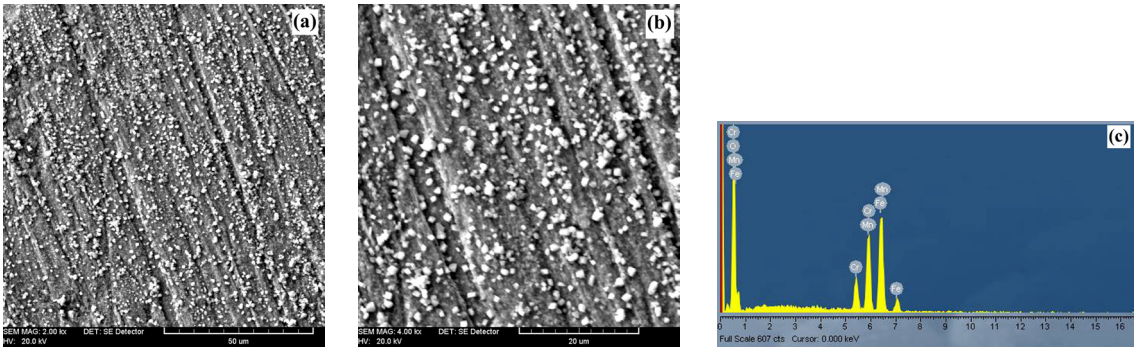

Fig. 5. Surface morphology of uncoated AISI 430 steel at magnification of (a) 2000X and (b) 4000X and (c) EDS point analysis after 200 hours oxidation in air at 800°C.

Fig. 6 shows surface morphology of Ni-Co-TiO_2 composite coating at two magnification of 500X (Fig. 6a) and 1000X (Fig. 6b) and EDS point analysis (c) after 200 hours oxidation in air at 800°C. The oxide formed on the surface of the coating has good adhesion to the substrate and was not removed from the surface. The oxide surface was also quite uniform. The surface of the Ni-Co-TiO_2-coated steel was completely different from that of the bare steel after 200 hrs of oxidation. Moreover, no spallation or cracks were observed on the oxidized surface of the Ni-Co-TiO_2-coated steel and the surface of the coated steel was covered with uniform and dense oxide scale.

EDS analysis (Fig. 6c) represents that the oxidized coating layer includes Ni, Co, Ti, Fe, Cr and O. Analysis by EDS indicated that Ni, Co, Ti, Fe, Cr and O contents in the composite coating were 24.4, 17.5, 5.2, 19.6, 7.8 and 25.5 wt.%, respectively.

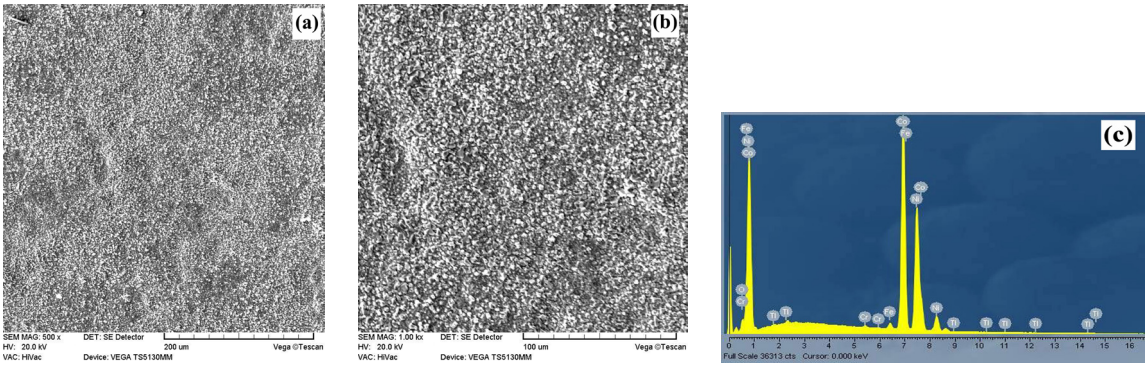

Fig. 6. Surface morphology of Ni-Co-TiO_2 composite coating at magnification of (a) 500X and (b) 1000X and (c) EDS point analysis after 200 hours oxidation in air at 800 °C.

Fig. 7 demonstrates XRD patterns of uncoated and Ni-Co-TiO_2 coated steel after 200 hours in air at 800°C. In uncoated samples Cr_2O_3, $MnCr_2O_4$, $FeCr_2O_4$, and Fe_2O_3 phases were identified (Fig. 7a). The formation of Cr_2O_3 is due to the outward diffusion of chromium and inward diffusion of oxygen [14, 15]. The presence of $MnCr_2O_4$ spinel is due to the presence of low amounts of manganese in this steel. This phase is observed in ferritic steels with a small amount of manganese, Ebrahimifar et al. concluded that the formation of the spinel phase on the chromium layer corresponds to a high coefficient of manganese ion penetration (DMn> DFe> DCr) [34].

When the alloy is subjected to the temperature range of 650-850°C the $(Mn,Cr)_3O_4$ spinel layer will be formed [35, 36]. $MnCr_2O_4$ spinel can be formed after the deposition of Cr_2O_3, which then reacts with MnO, through the following reaction:

$$Cr_2O_3 + MnO = MnCr_2O_4 \quad (4)$$

$MnCr_2O_4$ is thermodynamically more stable than both Cr_2O_3 and MnO [37-39]. $MnCr_2O_4$ spinel could reduce

significantly the vaporization pressure of gaseous chromium species but is non-protective [13].

The formation of FeCr2O4 is related to the reaction of FeO with Cr_2O_3 [14, 36]. Also, the formation of Fe_2O_3 is due to the outward diffusion of Fe and inward diffusion of O [14, 15].

Fig. 7b shows the x-ray diffraction pattern of the Ni-Co-TiO_2-coated steel after 200 hours of oxidation at 800°C. In this analysis, oxides formed on the surface of coated steel consisted of NiFe2O4, $NiCr_2O_4$, $CoFe_2O_4$, $CoCr_2O_4$, $CoCrFeO_4$, Cr_2O_3, Fe_2O_3, NiO and TiO_2. The existence of these phases has been confirmed by other researchers 29, [38-40]. In oxidation of chromium-containing alloys, which oxidized in long times, two distinct layers will form [14, 15]. The interior layer is rich in chromium. The XRD analysis confirms the existence of Cr_2O_3 phase (Fig. 7b). The outer layer is rich in nickel and according to the XRD analysis, the presence of the NiO phase in the second layer is definite. The Ni-Co-TiO_2 composite coating after oxidation to the Fe_2O_3/$NiFe_2O_4$/$CoFe_2O_4$ layer, which is chrome-free, has been transformed into a chromium-rich oxide layer. The spinel $NiFe_2O_4$ and $CoFe_2O_4$ prevent chromium intrusion and also improve the adhesion of the composite coating to the substrate [32, 41].

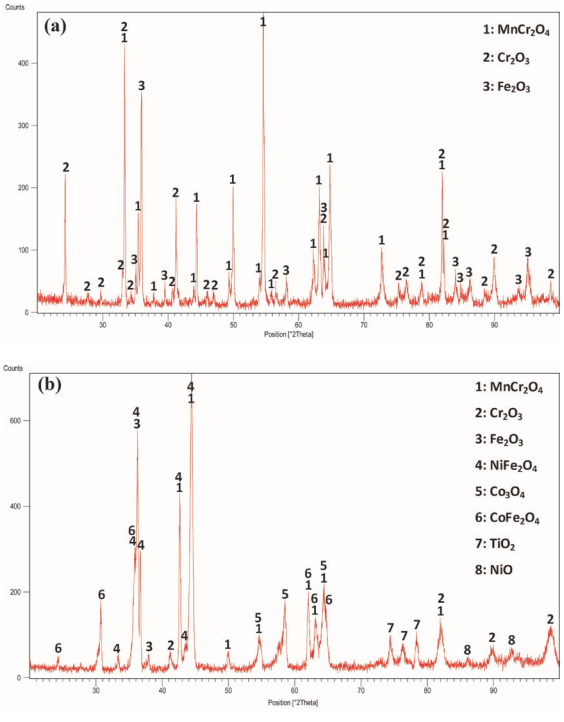

Fig. 7. XRD pattern of (a) uncoated AISI 430 and (b) Ni-Co-TiO_2-coated steed after 200 hours of oxidation.

The intensity of chromia phase in XRD pattern of coated sample is lower in comparison with the uncoated one. It is clear that, the coating layer prevent inward diffusion of oxygen, leading to retention growth of the Cr_2O_3 layer. Consequently, the oxidized Ni-Co-TiO_2 layer that was developed on an inner Cr_2O_3 layer, the Cr volatilization is prevented. The previous work [42] illustrated that, metallic coatings of Co, Cu and Ni on Crofer 22 APU with a thickness of about 10 µm showed good retention of Cr volatilization.

3. 2. 2. Cyclic Oxidation Resistance

Fig. 8 shows the weight gain of specimens as a function of cycle number. In all of the cycles the Ni-Co-TiO_2 composite coated specimens had less mass gain compared with uncoated ones. It refers to the protective spinels that limit the oxidation reactions [14, 15]. The weight gain for uncoated and coated specimens were obtained 1.852 mg cm^{-2} and 1.068 mg cm^{-2} respectively after 50 cycles. Fig. 9 shows square of weight gain as a function of cycle number during cyclic oxidation for Ni-Co-TiO_2 coated and uncoated samples. The lower Kp value for Ni-Co-TiO_2 coated samples (8.555×10^{-12} g^2 cm^{-4} s^{-1}) than uncoated samples (7.555×10^{-11} g^2 cm^{-4} s^{-1}) during the cyclic oxidation shows the positive role of Ni-Co-TiO_2 composite coating layer.

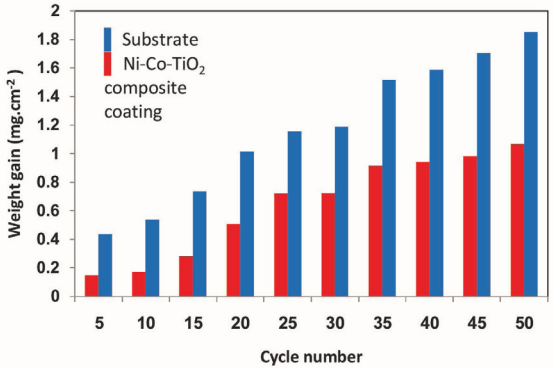

Fig. 8. Weight gain as a function of cycle number during cyclic oxidation for Ni-Co-TiO_2 coated and uncoated samples.

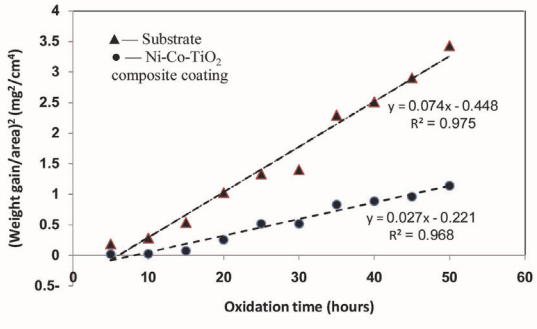

Fig. 9. Square of weight gain as a function of cycle number during cyclic oxidation for Ni-Co-TiO_2 coated and uncoated samples.

Fig. 10 shows surface morphology of uncoated sample after 50 cycles of oxidation in air at 800oC at two magnification of 500X (fig. 10a) and 2000X (fig. 10b). The oxidized surface demonstrated non-uniform surface with large spallation and cracks.

Fig. 11 shows surface morphology of Ni-Co-TiO_2 composite coating after 50 cycles of oxidation in air at 800°C at two magnification of 500X (Fig. 10a) and 1000X (fig. 10b). The surface of Ni-Co-TiO_2 composite coated specimens after cyclic oxidation was uniform with no porosity, spallation and no crack.

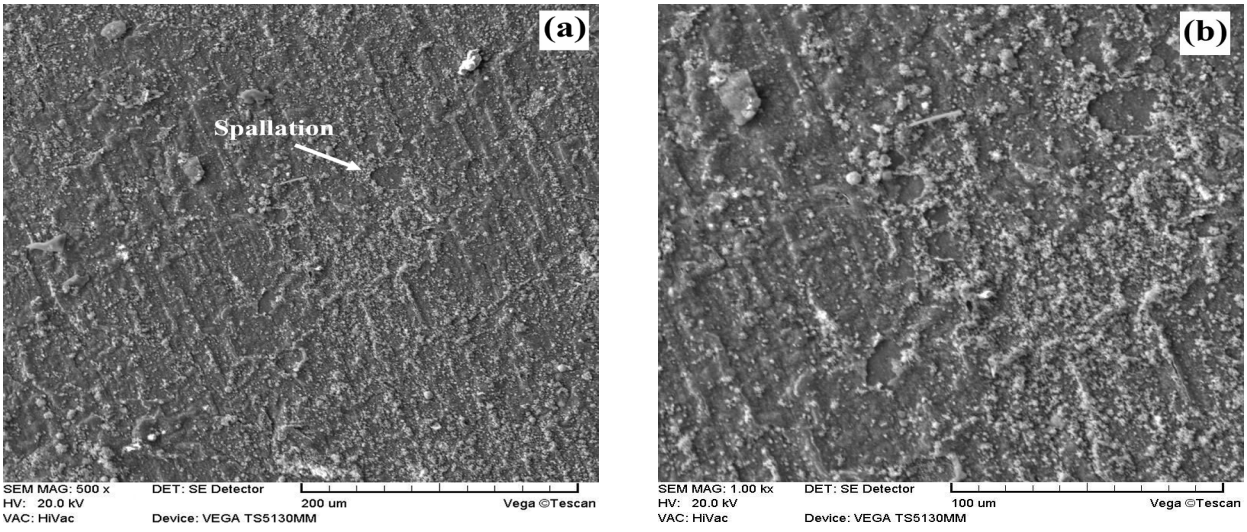

Fig. 10. Surface morphology of uncoated AISI 430 steel after 50 cycles of oxidation in air at 800°C at magnification of (a) 500X and (b) 1000X.

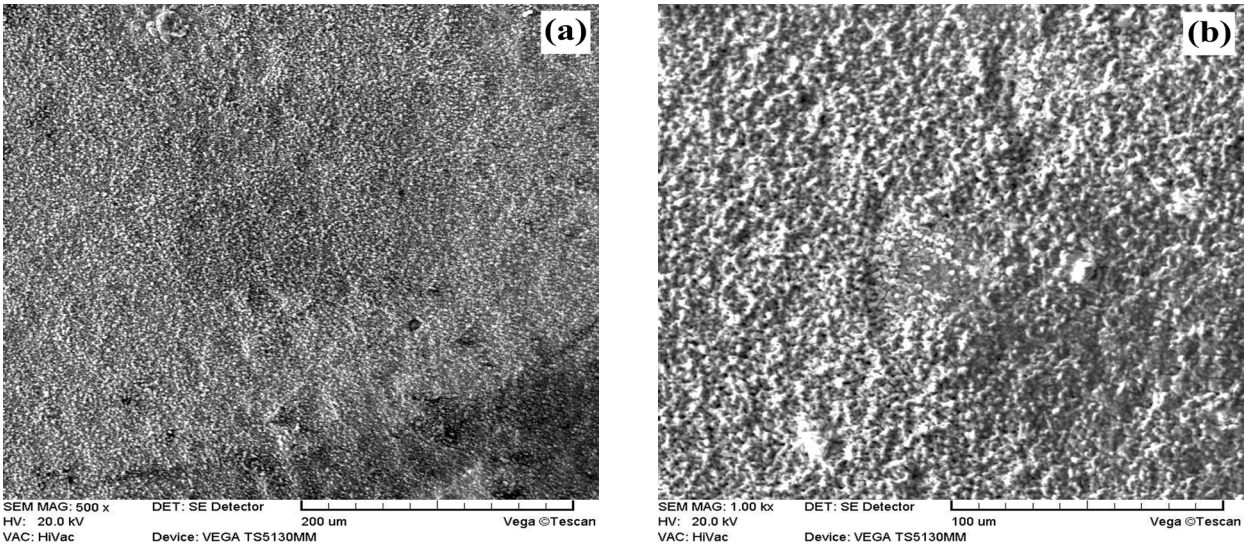

Fig. 11. Surface morphology of Ni-Co-TiO_2 composite coating after 50 cycles of oxidation in air at 800°C at magnification of (a) 500X and (b) 1000X.

After 50 cycles, the coating layer had good adherent to the substrate while the uncoated specimen surface spalled in some areas. Spallation and cracking are the result of the thermal expansion coefficient mismatching of the oxide, or coating layer with the substrate [14, 15].

The created cracks in the surface of bare steel are likely related to stresses originating from differences in thermal expansion coefficient between the substrate and the formed oxides on the surface. Thermal expansion coefficient of iron oxides is larger than that of the stainless steel, resulting in tensile stresses in the oxide during cooling [43].

The spalled scale creates a diffusion path for cations and anions. Therefore, the simple migration of ions allows the oxide layer to grow at a higher rate [34, 36].

4. Conclusions

Ni-Co-TiO_2 composite coating was electrodeposited on the AISI 430 austenitic stainless steel to improve the oxidation resistance.

The lower values of weight gain during oxidation tests were because of the more oxidation resistance.

The formation of Ni-Co Spinels during oxidation tests at 800ºC decreased the chromia growth by limiting the outward diffusion of Cr cation and inward diffusion of oxygen anion and it cussed the lower weight gain (1.229 mg cm^{-2}) compared to the bare samples in isothermal oxidation (2.052 mg cm^{-2}).

In cyclic oxidation the coated samples exhibited a good resistance against spallation and cracking and it led to the lower values of weight gain (1.068 mg cm^{-2}) compared to uncoated samples (1.852 mg cm^{-2}) after 50 cycles of oxidation.

References

[1]K. Huang, P.Y. Hou and J.B. Goodenough: Ionics., 129 (2000), 237.
[2]S.P.S. Badwal, R. Deller, K. Foger, Y. Ramprakash and J.P. Zhang: Ionics., 99(1991), 297.
[3]M.C. Tucker, H. Korokawa, C.P. Jacobson, L.C. De-Jonghe and S.J. Visco: J. Power Sources., 160 (2006), 130.
[4]S.P. Jiang, J.G. Love and L. Apateanu: Ionics., 160 (2003), 15.
[5]Y. Matsuzaki and I. Yasuda: Ionics., 132 (2000), 271.
[6]X. Chen, P.Y. Hou, C.P. Jacobson, S.J. Visko and L.C. De Jonghe: Ionics., 176(2005), 425.
[7]Z. Yang, G. Xia, S.P. Simner and J.W. Stevenson: J. The Electrochemical. Soc., 152(2005), 1896.
[8]Z. Yang, G. Xia, X. Li and J.W. Stevenson: J. Hydrogen Energy., 32(2007), 3648.
[9]Z. Yang, G. Xia and J.W. Stevenson: Electrochemical and Letters., 8 (2005), A168.
[10]W. Wei, W. Chen and D.G. Ivey: Chemistry. Mater., 19(2007), 2816.
[11]M.R. Bateni, P. Wei, X. Deng and A. Petric: Surf. Coat. Tech., 201(2007), 4677.
[12]P. Wei, X. Deng, M.R. Bateni and A. Petric: Corros., 63(2007), 529.
[13]H. Ebrahimifar and M. Zandrahimi: Oxid. Met., 84 (2015), 329.
[14]H. Ebrahimifar and M. Zandrahimi: Oxid. Met., 84 (2015), 129.
[15]E. Khoran, M. Zandrahimi, H. Ebrahimifar, Oxid. Met., 91 (2019), 177.
[16]S. Spanou, AI. Kontos, A.Siokou, AG. Kontos, N. Vaenas, P. Falaras and EA. Pavlatou: Electrochimica. Acta., 105(2013) 324.
[17]D. Thiemig and A. Bund: Surf. Coat. Tech., 202(2008), 2976.
[18]H. Gül, F. Kılıc¸ S. Aslan, A. Alp and H. Akbulut: Wear., 267(2009), 976.
[19]Y. Sun, IF. Kabulska and J. Flis: Mater. Chemistry and Physics., 145(2014) 476.
[20]M. Alizadeh, M. Mirak, E. Salahinejad, M. Ghaffari, R. Amini and A. Roosta: J. Alloys and Compounds., 611(2014), 161.
[21]Y. Yang and YF. Cheng: Electrochimica. Acta., 109(2013), 638.
[22]P. Wang, YL. Cheng and Z. Zhang: J. Coat. Tech., 8(2011), 409.
[23]H. K. Lee, HY. Lee and JM. Jeon: Surf. Coat. Tech., 201(2007), 4711.
[24]M. H. Fini and A. Amadeh: Transactions of the Nonferrous. Met .Soc., 23(2013), 2914.
[25]H. J. Zhang, YB. Zhou and JF. Sun: Transactions of the Nonferrous Metals. Soc., 23(2013) , 2011.
[26]IU. Haq and TI. Khan: Surf. Coat. Tech., 205(2011), 2871.
[27] G. Gyawali, SH. Cho and SW. Lee: Mater. Int., 19(2013), 113.
[28]S. Geng, S. Qi, Q. Zhao, S. Zhu and F. Wang: International. J. Hydrogen Energy., 37(2012), 10850.
[29]IU. Haq, K. Akhtar, Ti. Khan and AA. Shah: Surf. Coat. Tech., 235(2013), 691.
[30]L. Ma, KC. Zhou, ZY. Li and QP. Wei: J. Central South University of Tech., 17(2011), 708.
[31]S. Geng, Y. Li, ZH. Ma, L. Wang, L. Li and F. Wang: J. Power Sources., 195(2010) , 3256.
[32]S. Geng, S.Qi, D. Xiang, S. Zhu and F. Wang: J. Power Sources., 215(2012), 274.
[33]H. Ebrahimifar and M. Zandrahimi: Surf. Coat. Tech., 206(2011), 75.
[34]B. Nikrooz, M. Zandrahimi and H. Ebrahimifar: J. Sol Gel. Sci. Tech., 63(2012), 286.
[35]H. Ebrahimifar and M. zandrahimi: Oxid. met., 75(2010), 125.
[36]P. Jian, L. Jian, H. Bing and G. Xie: J. Power Sources., 158(2006), 354.
[37]SK. Mitra, SK. Roy and SK. Bose: Oxid. Met., 34(1990), 101.
[38]SK. Mitra, SK. Roy and SK. Bose: Oxid. Met., 39(1993), 221.
[39]X. Deng, P. Wei, MR. Bateni and A. Petric: J. Power Sources., 160(2006), 1225.
[40]F. Kılıç, H. Gül, S. Aslan, A. Alp and H. Akbulut: Colloids and Surf. A. Physicochemical and Eng., 419(2013), 53.
[41]M. Stanislowski, J. Froitzheim, L. Niewolak, WJ. Quadakkers, K. Hilpert, T. Markus and L. Singheiser: J. Power Sources., 164(2007), 578.
[42]J. Zurek, E. Wessel, L. Niewolak, F. Schmitz, TU. Kern, L. Singheiser and W.J. Quadakkers: Corros. Sci., 46(2004), 2301.